Effect of DC magnetic field on some physical and catalytic properties of Fe- and Fe/Pt- nanoparticles synthesized by BH method

E. D. Lefterova[1], A. E. Stoyanova[1*], H. Kolev[2], G. Tyuliev[2], D. Paneva[2],
G. R. Borisov[1], I. Dragieva[1]

[1]*Acad. Evgeni Budevski Institute of Electrochemistry and Energy Systems, Bulgarian Academy of Sciences, 1113, Sofia Bulgaria*
[2]*Institute of Catalysis, Bulgarian Academy of Sciences, 1113, Sofia Bulgaria*

The influence of dc magnetic field on some physical and catalytic properties of iron and platinum/iron nanoparticles is investigated. The nanoparticles are produced by a borohydride (BH) reduction process, as the dc magnetic field is applied during their synthesis. Structural differences between Fe powders are not observed. XRD and Mössbauer data show the presence of metallic iron and iron oxides (γ-Fe_2O_3/Fe_3O_4). In the Pt-Fe powders fcc-Pt and iron oxide-hydroxides are identified. XPS investigations confirm the availability of the iron oxides and metallic Pt. Pt^{2+} is identified too. A comparison of the XRD and the XPS data suggests the formation of core (metal)/shell (oxide) structure of the nanoparticles. The samples untreated with magnetic field show better electrocatalytic activities in PEM water electrolysis compared to the treated nanoparticles. For Pt-Fe samples, in which the iron content is about 50%, the influence of the magnetic field is weak. The observed effect can be explained with the influence of the magnetic field on the capability of their self-organization.

Key words: nanoparticles, borohydride (BH) reduction, PEM water electrolysis, XRD, XPS

INTRODUCTION

Iron oxide nano-particles are of considerable interest due to their wide range of applications. Nanotechnology has great potential and its development has allowed the synthesis of iron based nanoparticles with desired properties and expanded the range of their usage in different fields as magnetic recording, magnetic data storage devices, toners and inks for xerography, catalysts, sorbents, pigments, coatings, gas sensors, wastewater treatment[1], biomedical application, magnetic resonance imaging in medicine [2,3], etc. Ferrimagnetic particles are promising materials as sorbents in medical practice. Fe and $CoFe_2O_4$ nanoparticles can efficiently adsorb antigens, and viruses [4]; nanodispersive magnetite (Fe_3O_4) could be used for detoxification of cellular physiological fluids such as lymph or blood plasma [4-7]. Investigations on the use of magnetic nanoparticles for targeted drug delivery and for localized heating by absorption of electromagnetic radiation for efficiently eradication of cancerous cells are in progress [8-11].

Iron based materials are also cheap and efficient catalysts for many applications, as for the oxidation of CO, the oxidative pyrolysis of biomass, oxidation/reduction and acid/base reactions [12-15]. Iron oxide mixed with other metals has been shown to be a very active catalyst for the oxygen evolution reaction in water splitting, as well as other related processes. It is known that the best electrocatalyst toward oxygen evolution reaction among the pure metals is platinum. Alloying of Pt with various transition metals is often used in order to improve the catalytic activity toward the anodic reaction. It has been proven that carbon and Ti-oxide supported binary alloys of Pt with Fe and Co offer good performance mainly in direct methanol and polymer electrolyte fuel cells. The results obtained showed changes in particle size, distribution and electronic structure of the catalyst that are expected to be beneficial for catalytic activity of these materials toward the OER in water electrolysis as well [16-22].

It should be borne in mind that nano-particles of iron oxide are significantly more effective in many cases than conventional micron-sized iron oxide. These effects may arise from the high activity of the nano-particles having high surface areas and a better coordination of unsaturated sites on the

---

* To whom all correspondence should be sent:
E-mail: antonia.stoyanova@gmail.com

surfaces. Chemical and electronic properties, such as phase changes, OH content, band gap changes etc., could also have contributed to their high reactivity [23].

Furthermore, each application requires different material properties - thermal, chemical, and colloidal stability, magnetic characteristics, particle shape and size, and non-toxicity. These requirements determine the methods of preparation [1, 24]. With time the synthesis procedures for preparation of iron oxides in the nano range have gone through innovation, such as applying dc magnetic and electric fields that may set in a long-range ordering in the assembly and orientation during synthesis itself. The effect of magnetic field on the biomimetic synthesis, for example, leads to reduction in particle size and a directional assembly of synthesized super paramagnetic particles into a regular pattern in the protein film [25].

The aim of this work is to investigate the effect of the dc magnetic field applied during synthesis of iron and platinum/iron containing nanoparticles towards some physical and catalytic properties.

MATERIAL AND METHODS

Four samples containing Fe and Pt-Fe are prepared using the borohydride wet chemical reduction (BH) process with (marked with +) and without (-) dc magnetic field. The synthesis of the Fe nanoparticles is carried out with an aqueous solution of the salt $FeCl_2.4H_2O$, placed in the reactor with or without a dc magnetic field and reduced by addition of sodium borohydride solution under continuous stirring at 40°C for several min. The synthesis of the Pt-Fe nanoparticles required first synthesizing of platinum ethylenediamine complexes serving as metal precursors according to a previously developed preparation procedure [26, 27]. In a second stage, the prepared and mixed aqueous solutions of the precursors (Pt-complex and Fe-salt) are reduced by addition of sodium borohydride solution. After repeated washing of the obtained precipitate it was dried in a vacuum desiccator at room temperature.

Structural characterization was performed using XRD, XPS and Mössbauer spectroscopy. X-ray diffraction (XRD) patterns were recorded by X-ray diffractometer Philips APD15. The diffraction data were collected at a constant rate of 0.02 ^{o}.s^{-1} over an angle range of 2θ = 10 – 90 degrees with CuKα radiation (λ=1.54178 Å). The size of Pt crystallites was determined by the Scherrer equation [28]. The identification of crystalline phases was made by comparison with data on the JCPDS-ICDD files.

The Mössbauer spectra were obtained with an electromechanical spectrometer (Wissenschaftliche Elektronik GMBN, Germany) working in a constant acceleration mode. A 57Co/Rh (activity @50 mCi) source and α-Fe standard were used. The experimentally obtained spectra were subjected to mathematical processing according to the least squares method. The parameters of hyperfine interaction such as isomer shift (IS), quadrupole splitting (QS) and magnetic hyperfine field (Hhf), as well as the line widths (FWHM) and the relative spectral area (G) of the partial components of the spectra were determined. X-ray photoelectron spectroscopy measurements were performed on the ESCALAB MkII (VG Scientific) electron spectrometer at a base pressure in the analysis chamber of $5×10^{-10}$ mbar using twin anode MgKα/AlKα X-ray source with excitation energies of 1253.6 and 1486.6 eV, respectively. The peak fitting of the core-level XPS lines was carried out using Casa XPS Processing Software (Casa Software Ltd.) with a Gaussian–Lorentzian product function and a non-linear Shirley background [29]. The energy scale was calibrated by normalizing the C1s line of adsorbed adventitious hydrocarbons to 285.0 eV.

The electrochemical tests were performed on membrane electrode assemblies (MEAs) with a commercial polymer membrane Nafion 117 (Alfa Aesar), as an electrolyte. MEA was prepared by hot pressing of the electrodes for hydrogen (HER) and oxygen evolution (OER) on both sides of the membrane using a 5% Nafion solution as a binder. The electrodes with geometric area of 0.5 cm^2 had a double layered structure, consisting of a hydrophobic backing layer (GDL) and an active catalytic one (metal loading of 5 mg.cm^{-2}). The preparation procedure is described elsewhere [22].

The performance characteristics of the prepared MEA were investigated in a self made laboratory PEM electrolytic cell, consisting of two gas compartments where hydrogen and oxygen evolution take place, separated by the membrane electrode assembly under study. A reference electrode (commercial E-TEK catalyst containing 20% Pt on carbon support) was situated in the hydrogen evolution compartment. The catalytic activity of the prepared catalysts was studied using the techniques of cyclovoltammetry and steady state polarization at temperatures of 20°C and 80°C. All electrochemical measurements were carried out with a commercial galvanostat/potentiosat POS 2 Bank Electronik, Germany.

RESULTS AND DISCUSSION

For clarifying of the observed effects physical analyses were performed to trace the changes in the structure of the obtained nanoparticles with and without a magnetic field.

X-ray diffraction

The X-ray diffractograms of the synthesized Fe and Pt-Fe powders are presented in Figs. 1 and 2, respectively. XRD patterns of Fe powders (samples Fe(+) and Fe(-)) (Fig. 1) are almost identical. The phase analysis shows a presence of metallic iron (α-Fe) with crystallite size of 6 nm and iron oxides Fe_3O_4/γ-Fe_2O_3 with crystallite size of 8÷10 nm, respectively. X-ray diffractograms for Pt-Fe powders (samples Pt-Fe(+) and Pt-Fe(-)) are more complicated (Fig. 2a). No metallic iron (α-Fe) is registered, but fcc-Pt is additionally identified. Pt cell parameter was determined using a nonlinear regression analysis with the "UnitCell" software [30].The calculated cell parameters for Pt (3.920 and 3.919 Å) correspond to pure Pt (a=3.920 Å [31]). It means that there is no common Pt-Fe crystal cell. Hence, there is no alloying between

platinum and iron. The goethite (α-FeOOH) diffraction peaks are clearly distinguishable on the X-ray pattern of the sample synthesized with dc magnetic field. The broadened and strong peak at 2Θ ~53-54 degrees is connected with other iron hydroxide-feroxyhite (δ'-FeOOH)[32-34].
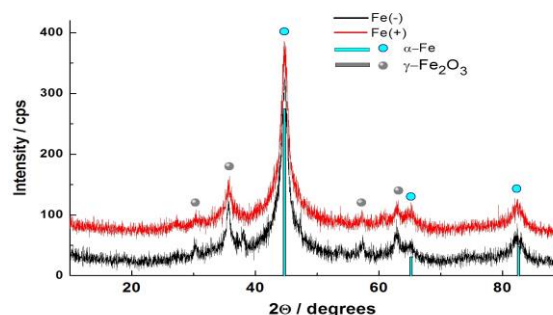

Fig. 1. XRD patterns of Fe nanopowders synthesized with Fe(+) and without Fe(-) magnetic field

The XRD 2Θ position of feroxyhite is presented with bargrams on Fig. 2. Some of these positions are close to or coincide with the positions of Fe_3O_4/γ-Fe_2O_3 and Pt. Hence, these peaks are superposition of sharper Pt (cryst. size 20 nm) or

Table1. Calculated Mössbauer parameters

| Sample	Components	IS, mm/s	QS, mm/s	H_{eff}, T	FWHM, mm/s	G, %
Fe(+)	Sx1 – Fe^0	0.03	-0.01	33.3	0.53	21
	Sx2 – Fe^0	0.06	-0.03	29.7	0.69	18
	Sx3 – Fe^0	0.06	0.00	26.1	0.77	26
	Sx4 – Fe^0	0.02	0.00	21.8	0.92	3
	Db – Fe^{3+}	0.33	0.78	-	0.52	32
Fe(-)	Sx1 – Fe^0	0.02	-0.01	33.3	0.53	21
	Sx2 – Fe^0	0.07	-0.03	29.5	0.69	21
	Sx3 – Fe^0	0.07	0.02	26.1	0.77	24
	Sx4 – Fe^0	0.04	0.00	21.8	0.92	4
	Db – Fe^{3+}	0.33	0.80	-	0.52	30
FePt(-), RT	Sx - γ-Fe_2O_3-HD	0.34	0.02	33.0	2.00	71
	Db – Fe^{3+}	0.36	0.70	-	0.53	29
FePt(+), RT	Sx1 - γ-Fe_2O_3	0.33	0.01	49.3	0.82	9
	Sx2 – α-FeOOH	0.34	-0.11	34.2	0.76	11
	Sx3 - α-FeOOH-HD	0.34	-0.11	27.7	1.86	44
	Db – Fe^{3+}	0.37	0.67	-	0.52	36
Pt-Fe(-), LNT	Sx1 - γ-Fe_2O_3	0.47	0.01	50.1	0.56	33
	Sx2 – γ-Fe_2O_3-HD	0.46	0.02	46.4	1.30	59
	Db – Fe^{3+}	0.45	1.02	-	0.90	8
Pt-Fe(+), LNT	Sx1 - γ-Fe_2O_3	0.47	0.05	49.1	0.60	30
	Sx2 – γ-Fe_2O_3-HD	0.48	0.07	47.2	0.48	15
	Sx3 - α-FeOOH	0.45	-0.10	44.5	0.74	25
	Sx4 - α-FeOOH-HD	0.45	-0.11	39.1	1.63	30
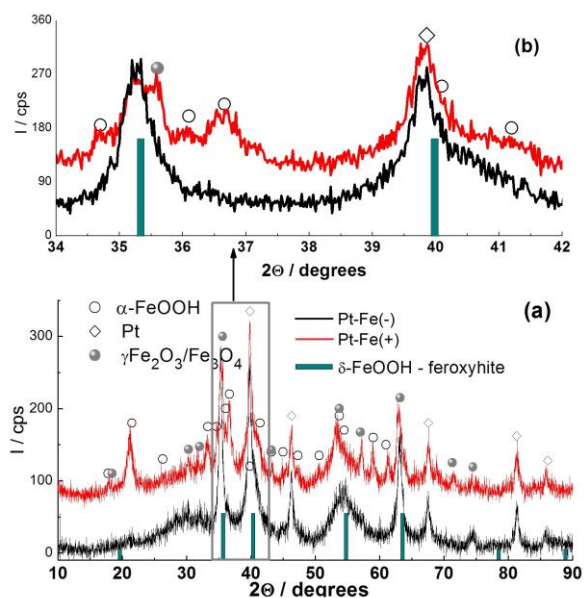
Fig. 2. XRD patterns of Pt-Fe nanopowders synthesized with (+) and without (-) magnetic field in the range (a) $2\Theta = 10 \div 90°$; (b) $\Theta = 34 \div 42°$.

$Fe_3O_4/\gamma\text{-}Fe_2O$ and broadened feroxyhite. This leads to additional broadening in the lower part, splitting and/or asymmetry of these peaks (Fig. 2b). The diffuse maximum between 22-32° 2Θ could be explained with ultra dispersed iron oxides.

Mössbauer spectroscopy

All Mössbauer spectra measured at room temperature consist of a pronounced doublet in the center and complex broadening and overlapping sextet components (Fig. 3).
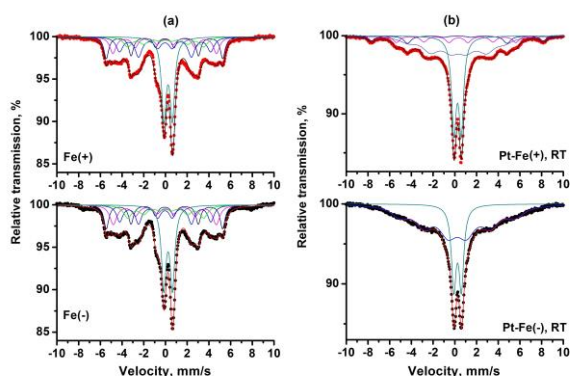

Fig. 3. Mössbauer spectra of Fe and Pt-Fe nanopowders synthesized with (+) and without (-) magnetic field, measured at room temperature (RT).

Both Fe samples (Fe(+) and Fe(-)) have similar Mössbauer spectra (Fig. 3a). The best mathematical processing is achieved using the model including 4 sextets and one doublet. Calculated Mössbauer

parameters are included in Table 1. All sextet components are due to Fe^0– isomer shift and quadrupole splittings are close to zero values. The different values of the effective magnetic field can be attributed to the components in which iron ions are neighbors of different chemical nature. The doublet is due to Fe^{3+} ions in octahedral coordination in the maghemite crystal structure.

The sextet components of Pt-Fe Mössbauer spectra (Fig. 3b.) obtained at room temperature are with stronger broadening and non-Lorenzian lines. For the sample Pt-Fe(-) the mathematical processing shows that Fe^{3+} ions in the octahedral coordination are incorporated into maghemite particles with different dispersity - a sextet for larger and a doublet for the smaller particles, respectively. The doublet with the same parameters could be connected with the presence of feroxyhite too [36]. Additional two sextets caused by octahedral coordinated Fe^{3+} ions with parameters of iron hydroxide - goethite with different dispersity are observed in the sample Pt-Fe(+), Sx2 for larger and Sx3 - HD to smaller particles. For a more detailed survey the Mössbauer spectra were measured at liquid nitrogen temperatures (LNT) (Fig. 4).
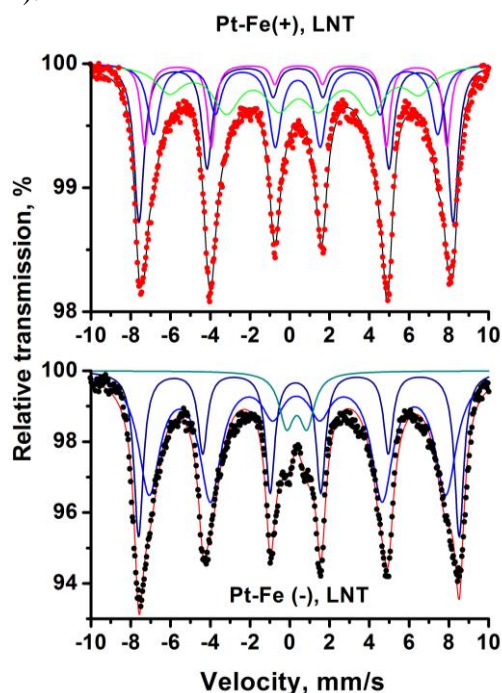

Fig. 4. Mössbauer spectra of Pt-Fe(+) and Pt-Fe(-) nanopowders, measured at liquid nitrogen temperature (LNT).

The lowering of temperature blocks the magnetic vector fluctuations induced by thermal motion and allows registration of superfine interactions in superparamagnetic materials. Both spectra at LNT contain mainly sextet components

with maghemite and goethite parameters. The introduction of the components of smaller and larger particles of the hydroxides and maghemite is connected with the particle size distribution in a very wide range.

X-ray photoelectron spectroscopy

Figure 5 presents high resolution of Fe2p core-shell spectra for all samples. There is no significant difference between the corresponding photoelectron spectra of the samples obtained with and without magnetic field. The Fe2p photoelectron spectra have a complex nature due to spin-orbital coupling, satellite structure and multiplet splitting of the oxidation states, as well as the low difference between Fe^{2+} and Fe^{3+} binding energies. But energy separation of the shake-up satellites is sensitive to the iron chemical state. Therefore, the satellite structure can be used to identify the oxide phases [36-37].
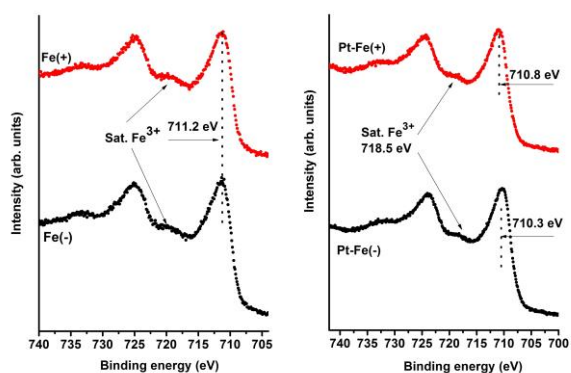
Fig. 5. High-resolution X-ray photoelectron spectra of Fe2p core-level.

In iron oxides the satellite located at ~8 eV (around 719 eV) above the main line is connected with Fe^{3+} while that at 714-715 eV is ascribed to the existence of Fe^{2+}. The registered Fe2p peaks at ~711, ~719, and ~725 eV represent the binding energies of Fe $2p_{3/2}$, shake-up satellite Fe $2p_{3/2}$ of Fe^{3+}, and Fe $2p_{1/2}$, respectively. The XPS study does not show the presence of Fe^0 on the surface of the samples. For samples Pt-Fe the Pt4f core-shell spectra (Fig. 6) confirm the availability of Pt in Pt^0 (~70.5 eV). The component at ~72.5 eV reveals additional Pt^{2+} states, most probably as $Pt(OH)_2$. The ratio Pt^0: Pt^{2+} is ~1:1 for both samples.

The O1s peak (Fig. 7) is fitted with three components: (1) the component situated at 529-530 eV is due to the oxygen in the Me-O bonds in FeO_x; (2) the component around 531-532 eV corresponds to Me–OH bonds; (3) the highest energy component (532.5-534 eV) can be assigned
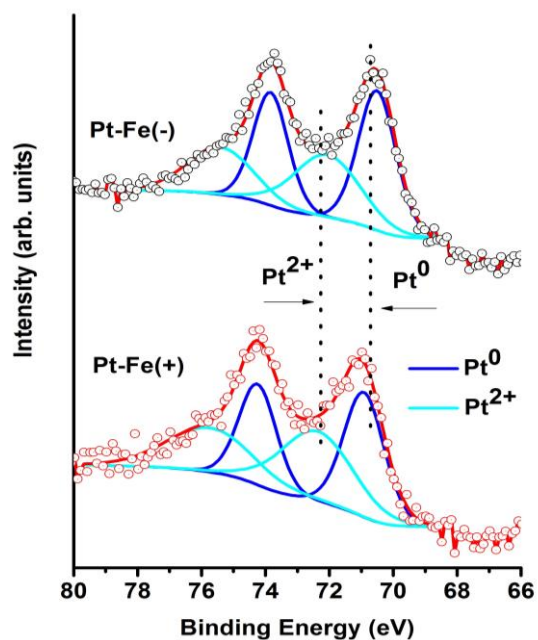
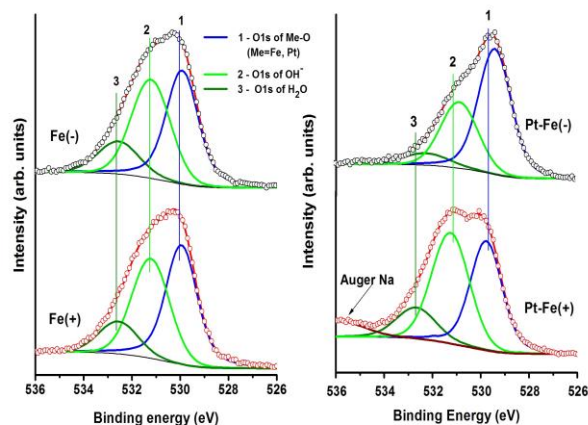**Fig. 6.** High-resolution X-ray photoelectron spectra of Pt4f core-level.

Fig. 7. High-resolution X-ray photoelectron spectra of O1s core-level.

to adsorbed H_2O and/or B-O bonds. Iron oxide-hydroxide (α-FeOOH) availability in sample Fe-Pt(+) reflects on the O1s peak. As a result, the component (2) dominates.

Electrochemical tests

The effect of the dc magnetic field applied during the synthesis is investigated towards the electrocatalytic properties of the Fe- and Pt-Fe-containing nanoparticles in PEM water electrolyses using cyclic voltammetry and steady state polarization techniques.

Cyclic voltammograms (CV) performed in the whole potential range between hydrogen and oxygen evolution give qualitative information about the nature of the processes occurring on the catalyst surface (Fig. 8).
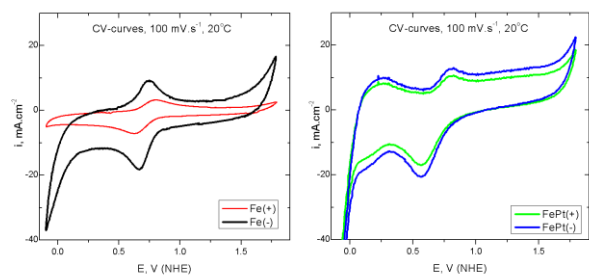
Fig. 8. Cyclovoltammetric curves of the samples under study at ascan rate of 100 mV.s^{-1} and temperature 20°C.

On the CV of the samples distinct, nearly reversible anodic and cathodic peaks situated in the potential range 0.7 – 0.75 V are observed. These peaks are due to the redox transition Fe^{3+}/Fe^{2+} and indicate an existence of Fe_3O_4/Fe_2O_3 phase [22]. In the unfolding of the potential in the opposite direction the cathode peak seems similar in shape and size at approximately the same values of the potential. The presence of these peaks means that in the cycling of the selected potential field, the catalytic material reversibly changes its valence state. For the Pt-based catalyst, peaks corresponding to hydrogen adsorption/desorption processes are situated in the potential range between 0.12 and 0.35 V (Fig. 8b) [19]. The shapes of the CV-curves of the catalysts treated and untreated with magnetic field are similar. The area (surface) of the curves of the untreated sample is greater in both cases, as in non-platinum-containing samples, it is essential. In iron-containing samples the difference in the active surface area is about 65%, while in the platinum-iron samples it is stationed around 18%. This result may be explained by the twice lower content of iron in the Pt-Fe composition and hence the much lower effect of the magnetic field. As may reasonably be expected, the active surface in a platinum-containing nanoparticle is higher in both cases.

The main results from the steady state electrochemical characterisation of the prepared catalysts, incorporated in MEAs are summarised in Fig. 9.
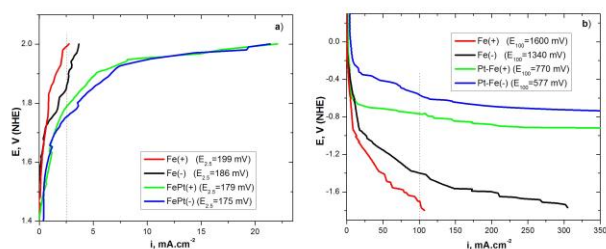

Fig. 9. Anodic (a) and cathodic (b) polarization curves of the samples under study at scan rate 1 mV.s^{-1} and temperature 80°C.

The polarization curves of the partial electrode reactions (OER and HER) involved in the electrolytic water splitting are recorded at a typical PEMWE operation temperature of 80°C. A significantly higher activity of the untreated catalyst to the magnetic field can be seen, as in the reaction of oxygen evolution, and in relation to that of the hydrogen evolution. The order of the catalytic activity for hydrogen and oxygen evolution of the studied composition is the following: Pt-Fe(-) > Pt-Fe(+) > Fe(-) > Fe(+). The influence of the magnetic field on the HER is more pronounced.

The observed effects can be explained with the influence of the magnetic field on the self-organization of the magnetic nanoparticles. Dragieva et al. [38-42] have observed self organization into chains of magnetic nanoparticles produced by the borohydride reduction method. The application of dc magnetic field during the synthesis reduces the space (pores) between the particles and densifies the chain structure. This leads to a decrease in the specific surface and hence, to a decrease in catalytic activity.

CONCLUSIONS

Structural studies showed no differences between Fe powders synthesized with and without dc magnetic field. A comparison of XRD, Mössbauer and XPS data suggests the formation of core (metal Fe)/shell (Fe-oxides) structure of the nanoparticles. In Pt-Fe powders Pt is in metal and oxide states. Iron is present mainly as Fe^{3+} ions in octahedral positions in the oxide and oxyhydroxide structures. The particles size distribution is within a very wide range.

It was found that the dc magnetic field applied during the synthesis of Fe- and Pt-Fe nanoparticles affects their electrocatalytic properties in PEM water electrolysis, as untreated samples showed a greater activity. In Pt-Fe compounds, in which the iron content is about 50% less, the influence of the magnetic field is weak. The observed effects can be explained with the influence of the magnetic field on the capability of their self-organization including the effects of the OH-groups.

REFERENCES

1. M. Mohapatra, S. Anand, *IJEST,* **2**, 127 (2010).

2. S. Mornet, S. Vasseur, F. Grasset, P. Veverka, G. Goglio, A. Demourgues, J. Portier, E.Pollert, E. Duguet, *Prog. Solid State Chem*., **34**, 237 (2006).

3. Lin M.M, Kim, H., and Mohammad M., *Nano Reviews*, **1**, 1 (2010).

4. Ю. Г. Яновский, *Технологии живых систем*., **4**, 73 (2007).

5. K. Cai, *Chem. Commun.* (Cambridge, U. K.), **27**, 7719 (2011).

6. M. Bhaumik, *J. Hazard. Mater.,* **186**, 150 (2011).

7. N. Y. Anisimova, F. S. Senatov, S. I. Milyaeva, M. V. Kiselevsky, *Medical Sciences*, **11**, 263 (2011).

8. D. Ho, X. Sun, S. Sun, *Acc. Chem. Res*., **44**, 875 (2011).

9. Q. A. Pankhurst, N. T. K. Thanh, S. K. Jones and J. Dobson, *J. Phys. D: Appl. Phys*., **42**, 224001. (2009)

10. I. Hilger, K. Fruhauf, W. Andra, R. Hiergeist, R. Hergt, W. A. Kaiser, *Academic Radiology*, **9**, 198 (2002).

11.C. H. Li, P. Hodgins, G. P. Peterson, *J. Appl. Phys*., **110**, 054303 (2011).

12. T. Miyata, Y. Ishino, T. Hirashima, *Synthesis* I, 834 (1978).

13. J. S.Walker, G. I.Stragauzzi, W. H. Manogue, G. C. A. Schuit, *J. Catal*., **110**, 298 (1988).

14. P. Li, D. Miser, S. Rabiei, R. Yadav, M. R.Hajaligol, *Appl. Catal. B: Environ*., **43**, 151 (2003).

15. P. Li, E. J. Shin, D. Miser, M. R. Hajaligol, F. Rasouli, B. In: Nanotechnology in Catalysis Zhou, S. Hermans and G.A. Somorjai (eds.), Kluwer Academic/Plenum, New York, 2004, p.515.

16. C. Medard, M. Lefˇevre, J.P. Dodelet, F. Jaouen, J. Lindbergh, *Electrochim. Acta,* **5**, 3202 (2006).

17. F. Charreteur, R. Stephane, J. Frederic, J. P. Dodelet, *Electrochim Acta*, **53**, 6881 (2008).

18. W. Li, X. Qin, Y. Yushan, *Int. J. Hydrogen Energy,* **35**, 2530 (2010).

19. S. Mukerjee, C. Srinivasan, M. Soriaga, *J. Electrochem Soc*., **142**, 1409 (1995).

20. W. Li, W. Zhou, H. Li, Zh. Zhou, B. Zhou, G. Sun, Q. Xin, *Electrochim. Acta,* **49**, 1045 (2004).

21. L. Xiong, A. Manthiram, *Electrochim. Acta,* **50**, 2323 (2005).

22. A. Stoyanova, G.Borisov,E. Lefterova, E.Slavcheva, *Int. J. Hydrogen Energy,* **37**, 16515 (2012).

23. P. Li, D. Miser, S. Rabiei, R. Yadav, M. R. Hajaligol, *Appl. Catal. B: Environ.* **43**, 151 (2003).

24. A. I. Martinez, M. A. Garcia-Lobato, D. L. Perry, In: Research in Nanotechnology Developments, Armando Barrañón (ed.), © Nova Science Publishers, Inc., 2009, p.183.

25. A. Sinha, S. Nayar, B.K. Nath, D. Dasb, P.K. Mukhopadhyayc, *Colloids and Surfaces B: Biointerfaces*, **43**, 7 (2005).

26. I. Dragieva, S. Stoeva, P. Stoimenov, E. Pavlikianov, K. Klabune, *Nanostruct. Mater*., **12**, 267 (1999).

27. I. Dragieva, S. Stoeva, P. Stoimenov, Z. Stoynov, Bg Patent No 103629 (03.08.1999).

28. J. Lanfgord, A. A. Wilson, *J. Appl. Crystallogr*., **11**, 102 (1978).

29 D. Shirley, *Phys. Rev. B*, **5**, 4709 (1972).

30. T. Holland, S. Redfern, *Mineral Mag*., **61**, 65 (1997).

31. JCPDS International Center for Diffraction Data, *Power Diffraction* File #87-0646.

32. V. A. Drits, B. A. Sakharov, A. Manceau, *Clay Minerals*, **28**, 209 (1993).

33. L. Carlson, U. Schwertmann, *Clays and Clay Minerals,* **28**, 272 (1980).

34. JCPDS International Center for Diffraction Data, *Power Diffraction File* # 13-0087

35. Mössbauer Spectroscopy: Tutorial Book, Yutaka Yoshida, Guido Langouche (eds.), Springer-Verlag Berlin Heidelberg, 2013.

36. M. Aronniemi, J. Sainio, J. Lahtinen, *Surf. Sci*., **578**, 108 (2005).

37. M.C.Biesinger, B.Payne, A.Grosvenor, L.Lau, A. Gerson, R. Smart, *Appl. Surf. Sci.,* **257**, 2717 (2011).

38. I. Dragieva, D. Buchkov, D. Mehandjiev, M. Slavcheva, *J. Magn. Magn. Mater.*, **72**, 109,(1988).

39. I. Dragieva, M. Slavcheva, D. Buchkov, D. Mehandjiev, *J. Magn. Magn. Mater.*, **89**, 75(1990).

40. I. Dragieva, D. Mehandjiev, D. Buchkov, M. Slavcheva, *J. Magn. Magn. Mater.*, **83**, 460(1990).

41. D. Mehandjiev, I. Dragieva, *Journal of Magnetism and Magnetic Materials*, **101**, 167 (1991)

42. I. Dragieva, C. Deleva, M. Mladenov, *Monatshefte fur Chemie*, **133**, 807 (2002).

ВЛИЯНИЕ НА МАГНИТНОТО ПОЛЕ ВЪРХУ НЯКОИ ФИЗИЧНИ И КАТАЛИТИЧНИ СВОЙСТВА НА Fe- И Fe/Pt НАНОЧАСТИЦИ СИНТЕЗИРАНИ ПО БХ МЕТОД

Е. Д. Лефтерова[1], А. Е. Стоянова[1]*, Х. Колев[2], Г. Тюлиев[2], Д. Панева[2], Г. Р. Борисов[1], Й. Драгиева[1]

[1]Институт по електрохимия и енергийни системи «Евгени Будевски», Българска академия на науките, 1113, София, България
[2]Институт по катализ, Българска академия на науките, 1113, София, България

Постъпила на 3 март 2015 г.; коригирана на 5 септември 2015 г.

(Резюме)

Изследвано е влиянието на постоянно магнитно поле върху някои физични и каталитични свойства на наночастици, съдържащи желязо и платина/желязо. Наночастиците са синтезирани чрез борохидридна редукция, като магнитното поле е прилагано по време на синтеза. Не се регистрира разлика в структурата между Fe-праховете, синтезирани с и без магнитно поле. Рентгеновата дифракция и Мьосбауеровата спектроскопия показват наличие на железни оксиди (γ-Fe_2O_3/Fe_3O_4). В Pt-Fe праховете са идентифицирани fcc-Pt и железни оксиди-хидроксиди. Рентгеновата фотоелектронна спектроскопия (РФС) потвърждава наличието на железни оксиди и метална Pt, както и на ОН-групи. Допълнително е идентифицирана и Pt^{2+}. Анализирането на данните от структурните изследвания подсказва формирането на core/shell структура (метална сърцевина и оксидна обвивка) на наночастиците. Образците без приложено магнитно поле проявяват по-добра електрокаталитична активност при ПЕМ електролиза на вода, като неговото въздействие върху Pt-Fe проби, в които съдържанието на желязо е около 50%, е значително по-слабо изразено. Наблюдаваният ефект може да се обясни с влиянието на магнитното поле върху способността за самоорганизация на наночастиците.